

Plate-Specific Gain Map Correction for the Improvement of  
Detective Quantum Efficiency in Computed Radiography

by

Erich A Schnell

Medical Physics Graduate Program  
Duke University

Date: \_\_\_\_\_

Approved:

\_\_\_\_\_  
James T. Dobbins III, PhD, Supervisor

\_\_\_\_\_  
Ehsan Samei, PhD

\_\_\_\_\_  
Shiva Das, PhD

Thesis submitted in partial fulfillment of  
the requirements for the degree of Master of Science  
in the Medical Physics Graduate Program in the  
Graduate School of Duke University

2010

ABSTRACT

Plate-Specific Gain Map Correction for the Improvement of  
Detective Quantum Efficiency in Computed Radiography

by

Erich A Schnell

Medical Physics Graduate Program  
Duke University

Date: \_\_\_\_\_

Approved:

\_\_\_\_\_  
James T. Dobbins III, PhD, Supervisor

\_\_\_\_\_  
Ehsan Samei, PhD

\_\_\_\_\_  
Shiva Das, PhD

An abstract of a thesis submitted in partial  
fulfillment of the requirements for the degree  
of Master of Science in the Medical Physics Graduate  
Program in the Graduate School of Duke University

2010

Copyright by  
Erich A Schnell  
2010

## Abstract

The purpose of this work is to improve the NPS, and thus DQE, of CR images by correcting for pixel-to-pixel gain variations specific to each plate. Ten high-exposure open field images were taken with an RQA5 spectrum, with a sixth generation CR plate suspended in air without a cassette. Image values were converted to exposure, the plates registered using fiducial dots on the plate, the ten images averaged, and then high-pass filtered to remove low frequency contributions from field inhomogeneity. A gain-map was then produced by converting all pixel values in the average into fractions with mean of one. The resultant gain-map of the plate was used to normalize subsequent single images to correct for pixel-to-pixel gain fluctuation. The normalized NPS (NNPS) for all images was calculated both with and without the gain-map correction. The NNPS with correction showed improvement over the non-corrected case over the range of frequencies from  $0.15 - 2.5 \text{ mm}^{-1}$ . At high exposure (40 mR), NNPS was 50-90% better with gain-map correction than without. A small further improvement in NNPS was seen from careful registering of the gain-map with subsequent images using small fiducial dots, because of slight misregistration during scanning. CR devices have not traditionally employed gain-map corrections common with DR detectors because of the multiplicity of plates used with each reader. This study demonstrates that a simple gain-map can be used to correct for the fixed-pattern noise and thus improve the DQE of CR imaging. Such a method could easily be implemented by manufacturers because each plate has a unique bar code and the gain-map could be stored for retrieval after plate reading. These experiments indicated that an

improvement in NPS (and hence, DQE) is possible, depending on exposure level, over all frequencies with this technique.

## **Dedication**

This work is dedicated to my wonderful parents, who have continued to support me in all my endeavors.

# Contents

Abstract .....	iv
List of Figures .....	ix
Acknowledgements .....	x
1. Introduction .....	1
1.1 Computed Radiography .....	1
1.2 DQE and image quality analysis .....	3
1.3 Digital image generation .....	5
2. Materials and Methods.....	7
2.1 Experimental Setup .....	7
2.2 Generation of the Gain Map .....	8
2.2.1 Beam Spectrum .....	8
2.2.2 Generation of the calibration curve .....	9
2.2.3 Correcting for beam inhomogeneity.....	10
2.2.4 Normalization .....	10
2.2.5 Alignment.....	10
2.2.6 Application of the correction .....	11
2.3 MTF analysis .....	11
2.4 Noise power spectrum analysis .....	12
2.5 Comparative tests to evaluate performance .....	14
2.6 Variation across different readers .....	15

3. Results.....	16
3.1 Uncorrected Flat Field Image.....	16
3.2 Gain map images and properties .....	17
3.3 Resultant flat field image after correction.....	18
3.4 Comparative NNPS improvement.....	19
3.5 Variations in improvement for different conditions .....	20
3.5.1 Varied Exposure .....	20
3.5.2 Varied Voltage .....	21
3.5.3 Alignment of image to be corrected with the gain map .....	22
3.5.4 Number of images used to generate the gain map.....	23
3.6 MTF evaluation.....	24
3.7 Variation across different readers .....	25
4. Discussion .....	29
5. Conclusion .....	34
Bibliography .....	35

## List of Figures

Figure 1: Single uncorrected flat field image. ....	16
Figure 2: Gain map.....	17
Figure 3: Resultant flat field image after correction.....	18
Figure 4: Normalized noise power spectrum for the single image in figure 1 and the gain map corrected image in figure 3. ....	19
Figure 5: Comparison of DQE improvement factor for differing orders of magnitude for exposure. ....	20
Figure 6: Comparison of DQE improvement factor for varied tube voltage and beam spectrum settings. ....	21
Figure 7: NNPS for an aligned and unaligned image correction. ....	22
Figure 8: Comparison of NNPS for corrected images using gain maps with 1, 2, 4 and 10 images in the average. ....	23
Figure 9: MTF comparison in the vertical and horizontal directions for single images and their corrected versions. ....	24
Figure 10: Subtraction of images read out on different readers of the same make, model, and condition.....	25
Figure 11: Image read out on the secondary reader corrected with gain map generated on the primary reader.....	26
Figure 12: Normalized noise power spectrum comparison in the horizontal direction between a corrected and uncorrected image read on the secondary reader. ....	27
Figure 13: Normalized noise power spectrum comparison in the vertical direction between a corrected and uncorrected image read on the secondary reader. ....	28

## **Acknowledgements**

I'd like to thank the following people for their help in the completion of this project:

Dr. James Dobbins for advising and guiding this work, as well as providing support in the most stressful times.

Dr. Ehsan Samei for his help in implementing the MTF analysis, as well as for serving on my committee.

Dr Shiva Das for serving on my committee.

Nicole Ranger, Dr. Maxwell Amurao, and Robert Ike for all their help in finding, accessing, and using vital equipment for this project.

Jered Wells, Matthew Freeman, and Brian Harrawood for technical and computer support.

# 1. Introduction

## 1.1 *Computed Radiography*

Computed radiography (CR) is a system for two dimensional radiograph acquisitions which uses reusable phosphor plates instead of traditional film. With use originating in the 1980's, CR is a mature modality which offers an easily integrated low cost system for filmless portable imaging. Today is it no longer the gold standard of radiographic systems, but it still offers several advantages over digital radiography in filmless departments. Flat panel detectors are the current gold standard for radiographs, but they come with some restrictions which CR can fill. Flat panels are mostly restricted to one per exam room, and can cost several times as much as a computed radiography system. Some flat panel bedside devices are becoming available, but they can be more easily damaged than CR plates in bedside applications. CR systems can service a huge number of rooms for bedside imaging thanks to its highly portable nature. The biggest downside of CR when compared to flat panel detectors is the image quality. Flat panel detectors produce a significantly better image, as measured by detective quantum efficiency (DQE) and are thus the preferred modality for most radiographic imaging. The goal of this work is to improve the image quality of CR systems using currently available hardware, bringing it closer to the level of flat panels. This improvement could improve its viability as a low cost modality, as well as improving the imaging standard in institutions like Duke that continue to use the system's utility as a bedside option.

CR plates come in several sizes, and are thin and lightweight for easy portability. The plates function by trapping holes formed in the phosphor layer of the plate in a metastable excited state when electrons are excited into the conduction band by incident x-rays. The plate, with the image thus stored, is placed into a reading device where it is exposed to an optical He/Ne scanning laser, which causes the trapped holes to be released so that they may decay, resulting in optical fluorescence which is then detected, generating a digital image<sup>10,13</sup>. The specifics of this process are discussed in the next section. Since the plates are sensitive to optical light after exposure, the plates are kept in cassettes which are opaque to visible light but cause little attenuation of the x-ray beam. The rigid cassettes also function as protection for the plates, which are flexible and can suffer damage with too much deformation.

The construction of the phosphor plate is fairly simple, with a layer of powdered barium fluorohalide sealed against a supportive backing. The exact structure and thickness, and thus the local gain of the imaging plate, however, fluctuate across the surface, and this fluctuation is unique to each plate. The result of this fluctuation is fixed pattern variation in the output response of the plate for a given exposure, which causes noise in the resultant image reducing its quality. The goal of this work is to prove the concept for correcting the gain fluctuations. A similar process is already done with flat panel detectors in digital radiography, which uses fixed detectors and immediate digitization rather than portable plates and a reader. The correction is much easier to

perform for flat panel detectors since the same scintillating layer is always used for images taken with a given detector, and the structure never shifts relative to the readout system.

This thesis proposes that it feasible to generate a gain map for each specific CR plate that the computer system could use to correct the digital output at the point of read-out. Each plate is already labeled with a specific serial number and bar code independent of the cassette which is used to identify the plates when they are read in ton associate them with a particular study. The variation for a particular plate is constant in time, so it would only need to be generated once to last the lifetime of the plate.

A gain map could be produced at the time of production by the manufacturer, and provided along with the plate already loaded into the reader system, or as a download into a pre-existing system. This would allow the improvement to be implemented clinically with no additional work by hospital staff.

## ***1.2 DQE and image quality analysis***

The noise power spectrum (NPS) for a given image is essentially a measure of the variance of image intensity, or noise, divided among the various frequency components of that image. This can be written mathematically as:

$$NPS(u, v) = \lim_{X, Y \rightarrow \infty} \frac{1}{2X \times 2Y} \left\langle \left| \int_{-X}^X \int_{-Y}^Y [I(x, y) - \bar{I}] e^{-2\pi i(ux+vy)} dx dy \right|^2 \right\rangle \quad (1)$$

where u and v are coordinates in frequency space, I is the image intensity,  $\bar{I}$  is the

average background intensity, and the angle brackets represent the ensemble average<sup>5</sup>, or the mean of the function across the possible states of the system. It is easy to see how equation 1 matches the description of the NPS as the variance of a particular frequency component. The normalized noise power spectrum or NNPS is just the noise power spectrum normalized by the square of the mean of the region being analyzed. In practice, NPS has several limitations. Regions of analysis have a finite size, and thus will pose limitations on the frequency sampling and frequency resolution of the NPS. Further, NPS measurements are very noisy, so a large number of measurements must be averaged to get any precision in the final measurement<sup>4</sup>.

Detective quantum efficiency, or DQE, is a measure of the efficiency of a detector system. It is defined by the effective number of quanta used by the device based on the signal to noise ratio, over the incident quanta of available data.<sup>7,8,11</sup> It is tedious to measure DQE directly, so in this project only the change in NPS will be measured. DQE is related to the inverse of the NPS as can be seen in equation 2, therefore a relative measured change in NPS due to a gain map correction is equal to the inverse of the relative change in DQE from that correction. DQE can be expressed as:

$$DQE(u, v) = \frac{MTF^2(u, v)}{NNPS(u, v) * SNR_{inc}^2} \quad (2)$$

where MTF refers to the modulation transfer function and  $SNR_{inc}$  refers to the signal-to-noise ratio for an ideal counter given the incoming number of photons<sup>5</sup>.

The modulation transfer function, or MTF, is another major contributor to the DQE<sup>7,12</sup>. The MTF is simply the amplitude of the Fourier transform of the point spread function (PSF), or in other words the spatial response of the detector to an incident delta function<sup>3</sup>. The MTF should be invariant with gain correction since we are not changing the fundamental spread response of the system.

### ***1.3 Digital image generation***

CR plate readers generate a digital image which is proportional to the log of exposure. This conversion uses several different settings and options at the time of readout which determines the details of the relationship. The first of these options, and one of the most important, is the “latitude” of an image. This essentially determines the range of exposures which are mapped to the range of digital values. Latitude 4 is the widest range, including all exposures, while lower values shrink the window, accentuating differences in the digital output. The sensitivity is another major factor in the readout, essentially adjusting the level of the window. This can either be set at a fixed level, or determined automatically by a pre-read, which is more prevalent clinically. The relation of exposure and digital output is given by:

$$\text{Log}(E) \propto -\frac{DPV \cdot L}{P_{max}} - \text{Log}(S) \quad (3)$$

where DPV is the digital pixel value, E is the exposure, Pmax is the maximum digital pixel value, L is the latitude, and S is the sensitivity, with the relation being linear. The

properties of this line, its slope and intercept, are known as the calibration factors for the reader, and are unique to the particular machine.

Readout settings are important since once an image is read it cannot be re-read from the plate accurately, since the physically stored information is lost in the process of fluorescing. To ensure full removal of information and prevent influence from one acquisition to the next, each plate is erased after readout by being bombarded by high intensity light in the scanner, which can be repeated as necessary.

## 2. Materials and Methods

### 2.1 *Experimental Setup*

For this study we used a single 6<sup>th</sup> generation Philips CR plate for all image acquisitions. The plate is 35.2cm by 42.8cm (about 14" by 17"). X-ray exposure was performed using a GE x-ray tube and generator. Images were read with a single Philips PCR Eleva CosimaX reader, which assigns 2140x1760 pixels to our plate, with a 12 bit data range for each pixel. All image acquisitions were taken at maximum latitude, four, with a fixed sensitivity of 200. For each image, the plate was suspended in air using a rig for reproducible positioning. The plate was mounted outside of the cassette to reduce the influence of the cassette on the generated gain map, thus all mounting and acquisitions were performed in the dark to avoid degrading the image. A ten minute waiting period (+- 30 seconds) was given after each exposure to minimize variation caused by temporal degradation of the image due to thermal decay. The plate was subjected to two extra erasures after each readout to ensure no data carried over after taking very high exposure images. Exposure measurements were done using a MDH model 1015 exposure meter, with a base uncertainty of (+-5%). The plate was mounted at a distance of 65.7 cm from the tube, and exposure measurements were made with the meter slightly behind the rig at 85.5cm from the tube. Exposure measurements were made free in air, and corrected for the inverse square effect to correspond to values at the plate surface.

## ***2.2 Generation of the Gain Map***

### **2.2.1 Beam Spectrum**

To generate the gain map for our plate, we took ten high exposure (~40mR), open field images. To ensure a reproducible beam, we used an International Electronics Commission 2005 RQA5 spectrum<sup>6</sup> beam with absolutely everything other than the aluminum removed from the beam, including the clear plastic tube cover on the collimator with the light field crosshair and the CR cassette. The goal was to limit any possible uncertainties such as scatter, and attenuation in the tube hardware. Initial tests showed that even the crosshairs painted on the collimator cover caused noticeable patterns in the resultant images. These ten images were converted to be linear to exposure, and then averaged. The result still included some information which was not specific to the plate itself, the most prevalent of which was the shading across the plate from the inhomogeneous x-ray beam.

RQA5 spectrum generation was performed by starting with a 70 kVp beam at 250mA and 21mm of Aluminum filtration in the beam. The requirement for RQA5 is that the mean transmission through the first 21mm of Aluminum must have a half value layer in Aluminum of 6.8mm. If the original settings do not show a 50% reduction in exposure with the addition of the 6.8mm, the kVp is adjusted up or down until the HVL requirement is met. While an exact 21mm of Aluminum filtration was available, the additional 6.8mm was not. To calibrate the RQA5 beam, then, we took measurements at

a variety of kVp values around 70 with thicknesses of Aluminum added which produced a reduction in exposure both greater than and less than 50%. We plotted the thickness of added aluminum vs. the log of the ratio of exposure with the added aluminum to that without for each kVp value. Since this plot is essentially linear for each voltage setting, we could see which voltage came closest to achieving a 50% reduction, had the required 6.8mm of extra aluminum been in the beam. 71kVp was determined to yield the most appropriate spectrum.

### **2.2.2 Generation of the calibration curve**

In order to be able to properly convert from digital image output from the reader to values linear with respect to exposure, in addition to the setting on the reader at the time of readout, we needed to measure the calibration curve values specific to the reader. To achieve this end, we used a narrow beam exposure at four different exposures at different orders of magnitude. We used exposures of 64mR, 6.3mR, .66mR and 0.062mR. To measure the exposure from a particular tube setting, we first set up our exposure meter in the beam and took three measurements at each setting to confirm the exposure delivered to the plate after inverse square correction. For the lowest exposure, we did ten shots at the intended tube setting in succession to bring the exposure up to a level our meter could properly measure. After taking the calibration images, we took the mean digital value from the center of the exposed area and used equation 1 to relate it to

the log of the exposure. By plotting the points from each of these four images, we generated the slope and intercept of the relation between pixel value and exposure.

### **2.2.3 Correcting for beam inhomogeneity**

To correct for the shading in the gain map we used a high pass filter on the image. The shading in the image exists at a very low frequency in Fourier space, so we used a very large kernel, 256x256 square, for our filter to remove the shading while minimizing the effect on the fixed pattern noise. Using such a large kernel means the filtered image will have strong edge effects as a result of the convolution, so to compensate we filtered a larger matrix with our image mirrored beyond its edges, and then cropped it back down to size after the convolution.

### **2.2.4 Normalization**

Once the filter is applied, the DC component (mean) of the original unfiltered average is restored. Once this is accomplished, the map is divided by that DC component to reach a mean value of unity. This allows the gain map to be applied to images without affecting the DC component.

### **2.2.5 Alignment**

Slight shifts in plate alignment as it is pulled through the reader system can have an effect on the registration of multiple acquisitions, specifically between an image and the gain map intended to correct it. To compensate for these alignment issues a fiducial alignment system was used in which the plate was marked with small black ink dots in

either corner, slightly displaced so vertical flips could be detected. These fiducial marks were used to register the ten images for the gain map before averaging, and were also used to align single acquisitions to the gain map before correction. The reader system is very accurate in dealing with the plates; no scaling factors were used, and the largest rotation used by our correction was 0.02 degrees.

### **2.2.6 Application of the correction**

Once the gain map for a specific plate is generated, the correction of any images from that plate is relatively simple. Once the image is converted to be linear to exposure, a simple pixel by pixel division of the original image by the gain map needs to be performed, since the map's mean is normalized to unity. This is the process we used in our work to perform the correction, though a more efficient correction method is possible. Since the log of a division is the difference between the log of the numerator and the log of the denominator, the gain map appropriately converted into logged space with the same values for latitude and sensitivity as a given image could correct that image directly in its original form via simple pixel by pixel subtraction.

### **2.3 MTF analysis**

To evaluate the MTF of the system, an opaque edge phantom was placed in the beam against the plate under our standard acquisition settings. The edge was placed near the center of the plate, and aligned both horizontally and vertically to evaluate both dimensions of the MTF. The edge itself is made of 250-microm-thick lead foil and is

intended to be opaque to the radiation. The program written by Ehsan Samei<sup>1,3</sup> looks at a small square region of the image traversed by the edge, converted to be linear to exposure. It looks at the response of the system to a very sharp delta-like edge to evaluate the one dimensional edge response function (ERF). The ERF is then differentiated to give the edge-response one dimensional line spread function (LSF), which is smoothed and then Fourier transformed to generate the one dimensional MTF as function of frequency. We compared the MTF in both dimensions for a single flat field image and for the same image corrected by our gain map in order to evaluate the effect gain correction would have on the response.

#### ***2.4 Noise power spectrum analysis***

To evaluate the quality of the images taken and the images after correction, we used a method for the calculation of the noise power spectrum developed by James T. Dobbins III in '94<sup>2,4</sup>. In order to compensate for the imprecision of the NPS measurement, we need to take multiple measurements from a single image.<sup>9</sup> To this end, we divided images into 64 ROI's from the central region of the image, each 128x128, and performed an NPS estimate on each one, averaging the results. Smaller ROI's allow for greater averaging out of the large variance associated with each measurement, but causes peaks in the NPS to be distorted by the low sampling. Larger ROI's avoid this sampling error, but reduced the number of ROI's available to average, causing greater variance. The outer border of the image is avoided for NPS calculation to avoid homogeneities near

the edges. 128x128 ROIs provide a good balance of frequency sampling and measurement precision. Each ROI is fit with a ramp function in x and y which is subtracted out to correct for non-uniformities. Each ROI has its 2D Fourier transform taken, and the resulting NPS is normalized by the square of the mean for the ROI in question to generate the normalized noise power spectrum (NNPS). Further refinement is done by correcting pixel values in each ROI by the square root of the mean pixel value relative to a standard ROI to account for slight intensity shading across the plate. The results for all the ROI's are then averaged to generate the final Normalized NPS of the image.

In order to perform comparison for image DQE, we needed to obtain a one dimensional plot of the NNPS from the two dimensional output. Values sampled directly from the u or v axes of the 2D NNPS are not representative of the amplitude of the NNPS near the axes, which is due to residual trending effects in the background. To obtain the one dimension plot, then, a thick slice of the 2D NNPS was taken in both directions, including four lines on each side of the axis but not including the axis itself. This is the IEC standard for generating a one dimensional NPS. The frequency of each location in these two slices was considered to be u and v added in quadrature. This gave a total of 1024 data points from which to draw the NNPS curve. The result was given additional smoothing by binning the data values into bins of  $0.05\text{mm}^{-1}$ . The one dimensional plot NNPS was the tool we used for comparison of our images.

When comparing the results of NNPS measurements with and without plate gain-map correction, we consider a value called the “DQE improvement factor”. This factor we define, as a function of frequency, as the ratio of the original NNPS(f) of an image to the NNPS(f) of that image corrected with a gain map. We label this value as DQE improvement rather than NNPS improvement since given a constant MTF and x-ray properties, DQE varies as the inverse of NPS as we mentioned in section 1.2. A DQE improvement factor of 1 indicates no change, while a factor of 4 would indicate a 4 fold improvement in DQE. This DQE improvement factor allows us to compute the effect on the detector DQE without actually measuring the DQE itself.

## ***2.5 Comparative tests to evaluate performance***

To judge the performance of our generated gain map, we corrected a variety of images taken under different settings and conditions and compared the DQE improvement factor for each. Tests we performed included comparing images at different exposure levels, which is important since lower exposures increase the amount of quantum noise relative to the fixed pattern noise, reducing the effect of the correction. Images were taken at 4.2mR and 0.4mR to compare to our base 42mR image. We also tested different beam voltages to gauge the effect that varied energy spectrum would have on the correction. Images were taken and corrected at 60kVp, 70 kVp, and 140 kVp without filtration at equivalent 42 mR exposure. The quality of the gain map performance was evaluated by comparing the level of improvement for gain maps

generated with varied numbers of images contributing to the average, including sets of one, two, four, and ten. Finally, we evaluated the level of improvement in NPS for an image registered to the gain map, versus one which was not.

## ***2.6 Variation across different readers***

To evaluate the contribution to image noise from variations arising due to the scanning process rather than the plate itself, images were acquired at 140 kVp and 42mR with no filtration, and read out in equal quantity using the primary reader and a second scanner of the same make, model, and operating conditions. A pixel-by-pixel subtraction was made between an image from each reader after converting to exposure to visualize the differences in artifact noise. Finally, an image from the secondary reader was corrected using the gain map generated on the primary reader, and the NNPS of the corrected and uncorrected image were obtained in both the horizontal and vertical directions to evaluate the quality of the correction.

## 3. Results

### 3.1 *Uncorrected Flat Field Image*

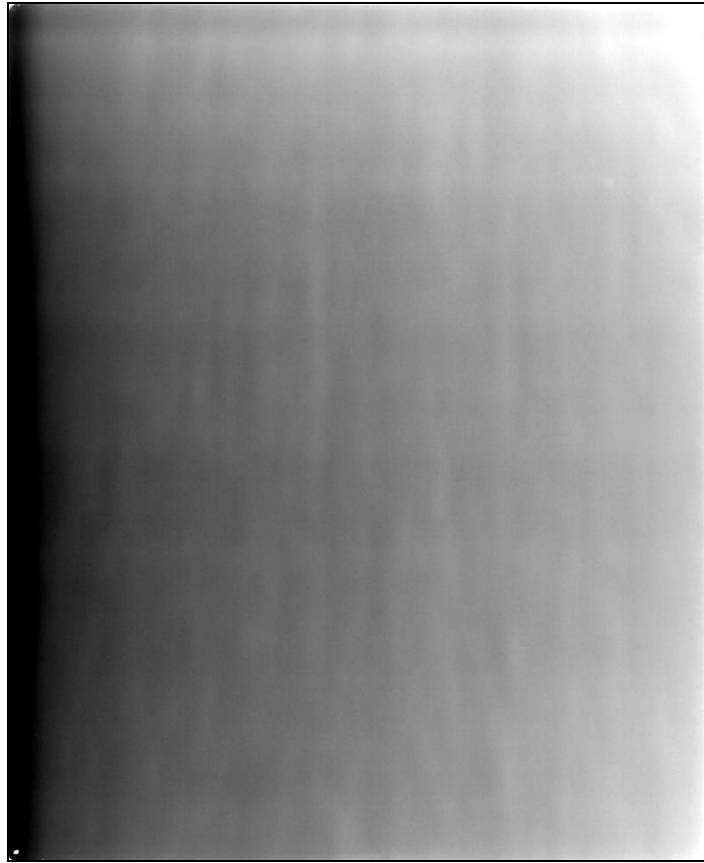


**Figure 1: Single uncorrected flat field image. Image was taken at an exposure of about 42mR. Important to note are the shading from the beam heel effect, as well as the medium frequency fixed pattern structure (seen as vertical streaks and mottle) we want to correct.**

Figure 1 shows a single high exposure image taken at around 42mR. Important to note is the medium frequency structure clearly visible in the image despite the very low quantum noise and the open beam, as well as the shading across the image from the anode heel effect of the beam. Also visible is one of the two fiducial marks in the bottom

left corner of the image. The image is displayed in digital output values, so dark corresponds to high exposure in this case.

### *3.2 Gain map images and properties*

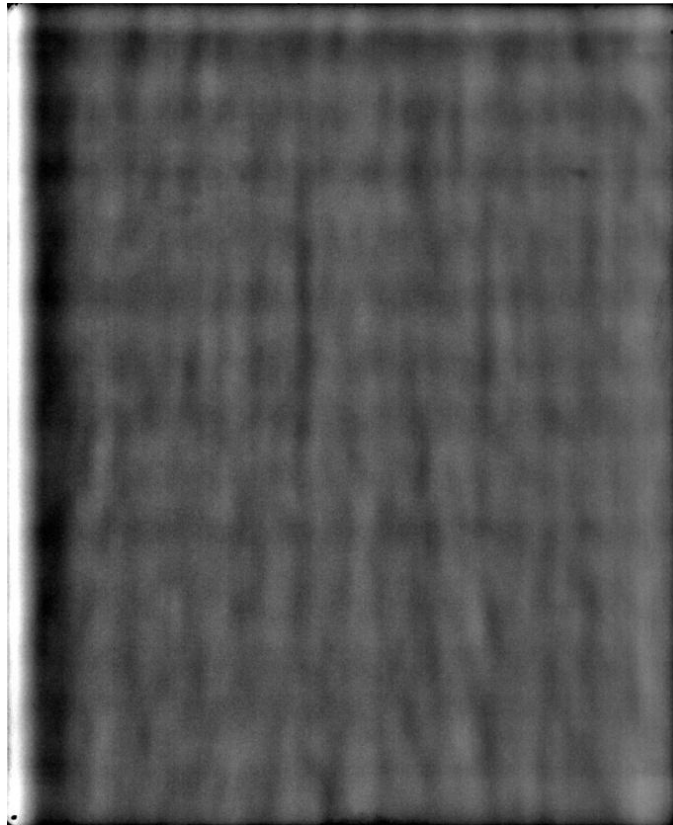


**Figure 2: Gain map. The gain map generated from ten aligned images similar to that in figure 1. Beam shading is largely removed, but fixed-pattern noise remains.**

The gain map produced by averaging ten aligned images such as the one in figure 1, can be seen in figure 2. Of note in the gain map itself is the remnants of some shading at the edges, especially in the horizontal direction. This is a result of both the mirroring method for preserving edge data during filtering, as well as incomplete filtering of the background shading from the gain map. The main body of the gain map

matches well the medium frequency noise seen in figure 1 without most of the background shading, which is exactly what we intended. The grayscale values for the structure is inverted in the gain map since it is created from images linear to exposure, rather than from images in the digital output space.

### ***3.3 Resultant flat field image after correction***

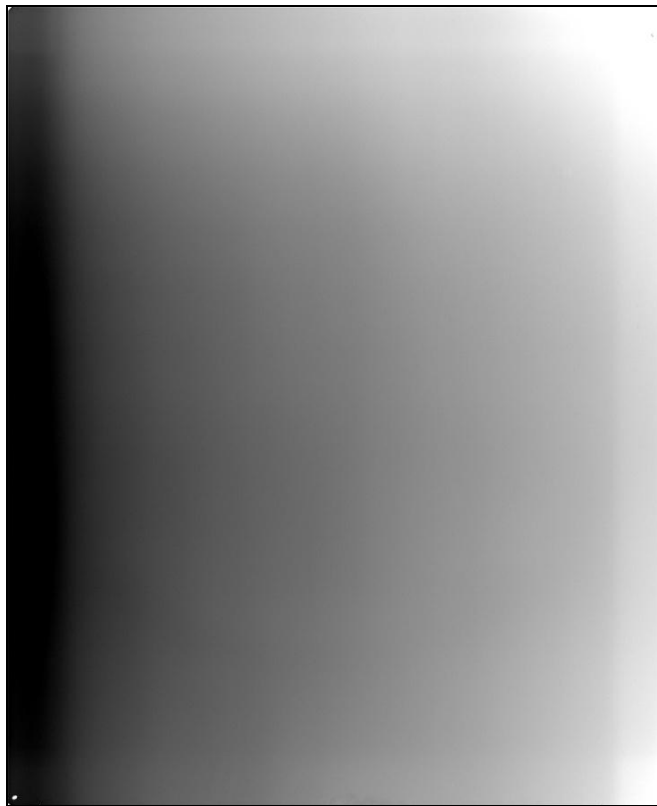


**Figure 3: Resultant flat field image after correction. Note the absence of structured noise compared to figure one, while retaining the shading of the beam.**

The image resulting from the correction of the original flat field image with the gain map is shown in Figure 3. The image is free of almost all of the fixed pattern noise, retaining only the very low frequency structure from the beam inhomogeneity as a

smooth, clear image. The image displays some edge effects carried over from the gain map itself as a result of the filtering method.

### 3.4 Comparative NNPS improvement

Figure 4 displays the normalized noise power spectra calculated for the image in figure 1 and the image in figure 3. The NNPS curve for the corrected image is clearly much lower on the power axis than the original. The improvement factor between the two, equivalent to the DQE improvement factor, is around 3 at the highest frequencies and increases to over ten at the lowest frequencies.

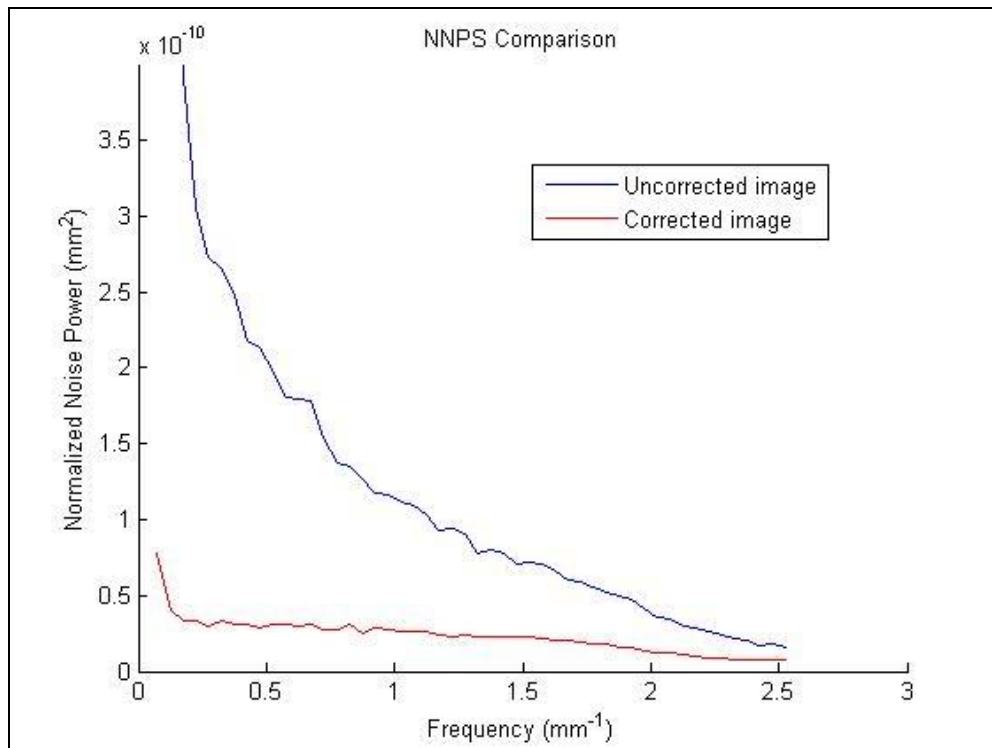


**Figure 4: Normalized noise power spectrum for the single image in figure 1 (blue) and the gain map corrected image in figure 3 (red). Improvement is smallest (factor of 3) at the highest frequencies and increases as frequency decreases, up to a factor of 10 and greater.**

The fixed pattern noise is most prominent in the low and mid frequencies, so it makes sense that the improvement would be best in those regions. The spike at very low frequencies is a result of the remaining very low frequency shading in the image.

### 3.5 Variations in improvement for different conditions

#### 3.5.1 Varied Exposure

The change in DQE improvement with varied exposure is the largest variation we encountered in the study. As expected, the improvement in NNPS was directly related to the incident exposure on the plate. Figure 5 displays the DQE improvement factor for 42mR, 4.2mR, and 0.4mR exposures using the same gain map in figure 2. The 42mR curve represents the improvement between the curves in figure 4.

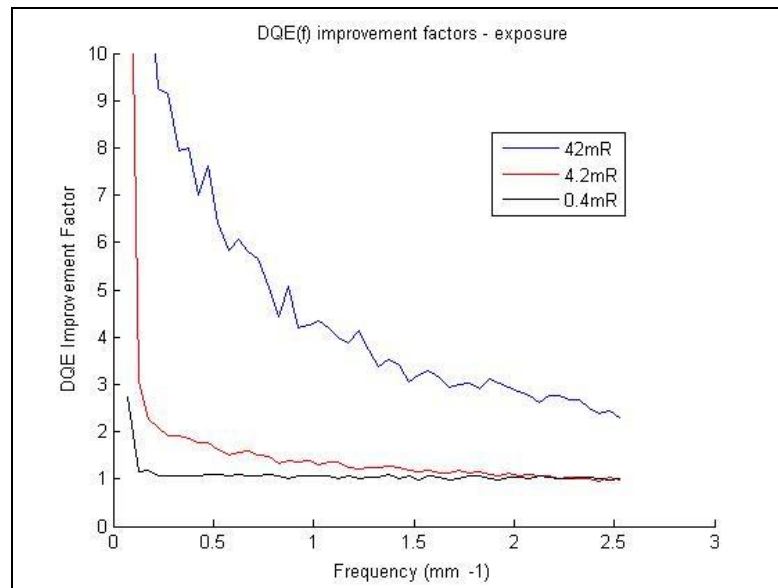


**Figure 5: Comparison of DQE improvement factor for differing orders of magnitude for exposure. Improvement decreases as exposure is reduced.**

The improvement is lower for the lower exposures as we might expect, offering improvement in only the medium to low frequencies in the 4.2mR exposure curve, starting at around a factor of three improvement at  $0.125\text{mm}^{-1}$  and declining down to about one at a frequency around  $2.2\text{mm}^{-1}$ . The 0.4 mR exposure offers the worst improvement, only showing any significant change at a few lower frequencies.

### 3.5.2 Varied Voltage

The tube voltage on the machine had some effect on the improvement factor for corrected images at constant exposure. The comparison of corrected images taken at 60, 70, 140 and 71 (RQA) kVp and 42mR is shown in figure 6.

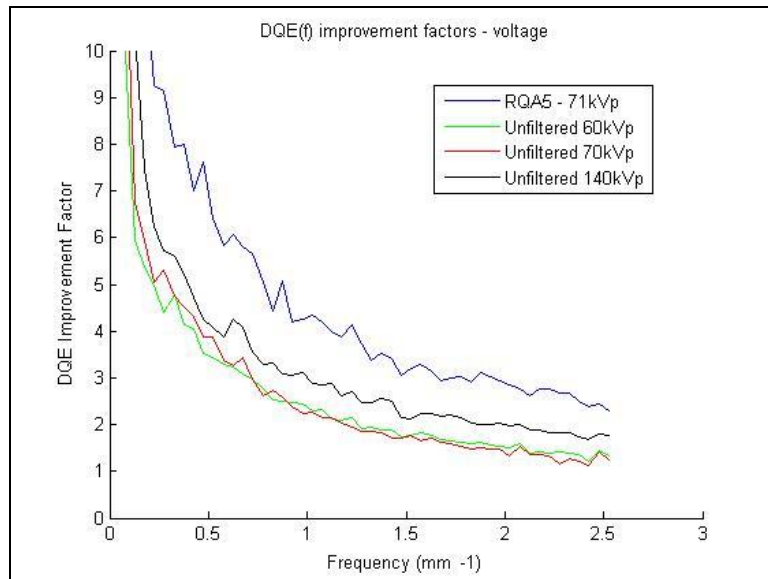


**Figure 6: Comparison of DQE improvement factor for varied tube voltage and beam spectrum settings. Exposure is constant at 42mR. Note that higher voltage tends to allow better correction, while the settings used to generate the gain map (RQA5) generate the best results.**

There is little difference between the 60 and 70 kVp images other than a slight improvement at lower frequencies for the 70kVp, as well as slightly varied fluctuations. The 140 kVp image showed consistently better improvement across the board compared to both 70 and 60 kVp. The RQA5 spectrum image had the best correction by quite a bit, which is due to the gain map being generated by images taken at the same beam spectrum.

### 3.5.3 Alignment of image to be corrected with the gain map

Aligning the image to be corrected with the gain map using the fiducial system provided a slight improvement in NPS in the corrected image, as can be seen in figure 7.

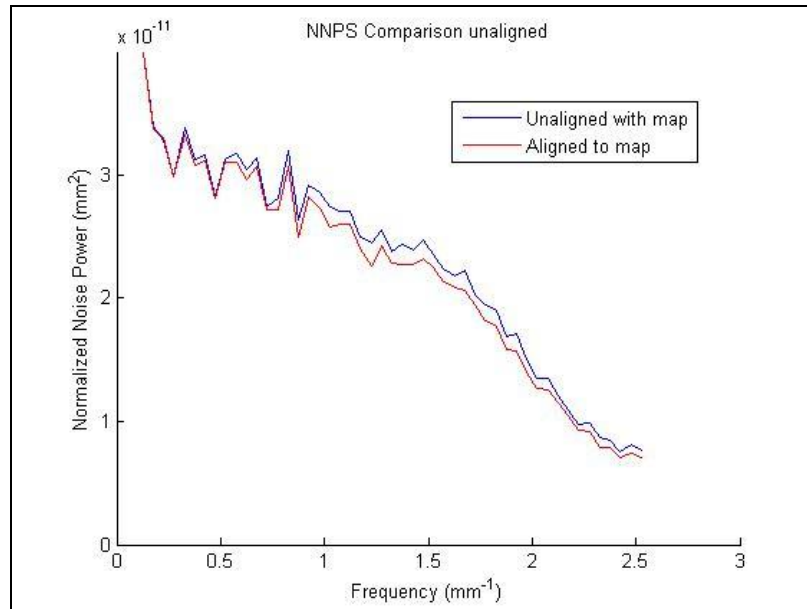


**Figure 7: NNPS for an aligned (red) and unaligned (blue) image correction. Best improvement is seen at medium frequencies. Note that the vertical axis is an order of magnitude smaller than in figure 4.**

The best improvements are seen at the medium frequencies, though even this improvement is minimal. Note that the axis for noise power in figure 7 is an order of magnitude smaller than used for figure 4.

### 3.5.4 Number of images used to generate the gain map

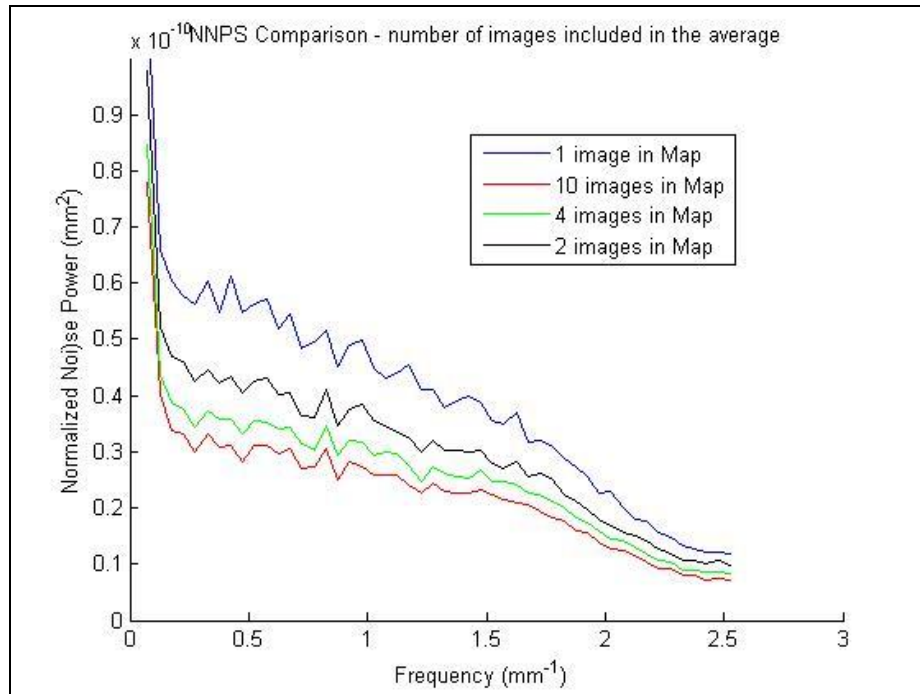


**Figure 8: Comparison of NNPS for corrected images using gain maps with 1 (blue), 2 (black), 4 (green) and 10 (red) images in the average. Note asymptotic approach to a minimum as the number increases.**

The NNPS of our corrected image improves as we increase the number of images used to generate the gain map, which can be seen in figure 8. The improvement seems to be an asymptotic approach towards a minimum NNPS spectrum at sufficiently large numbers of images. There was only a ~10% difference in the final NNPS curves going from 4 to 10 images in the average, indicating that an average of 10 is likely sufficient.

### 3.6 MTF evaluation

The MTF measurements showed that there was essentially no change in the MTF response of the system as a result of applying the gain map correction. The MTF comparison for the vertical and horizontal MTF can be seen in figure 9. This result justifies the use of NNPS improvement alone as the DQE improvement factor.

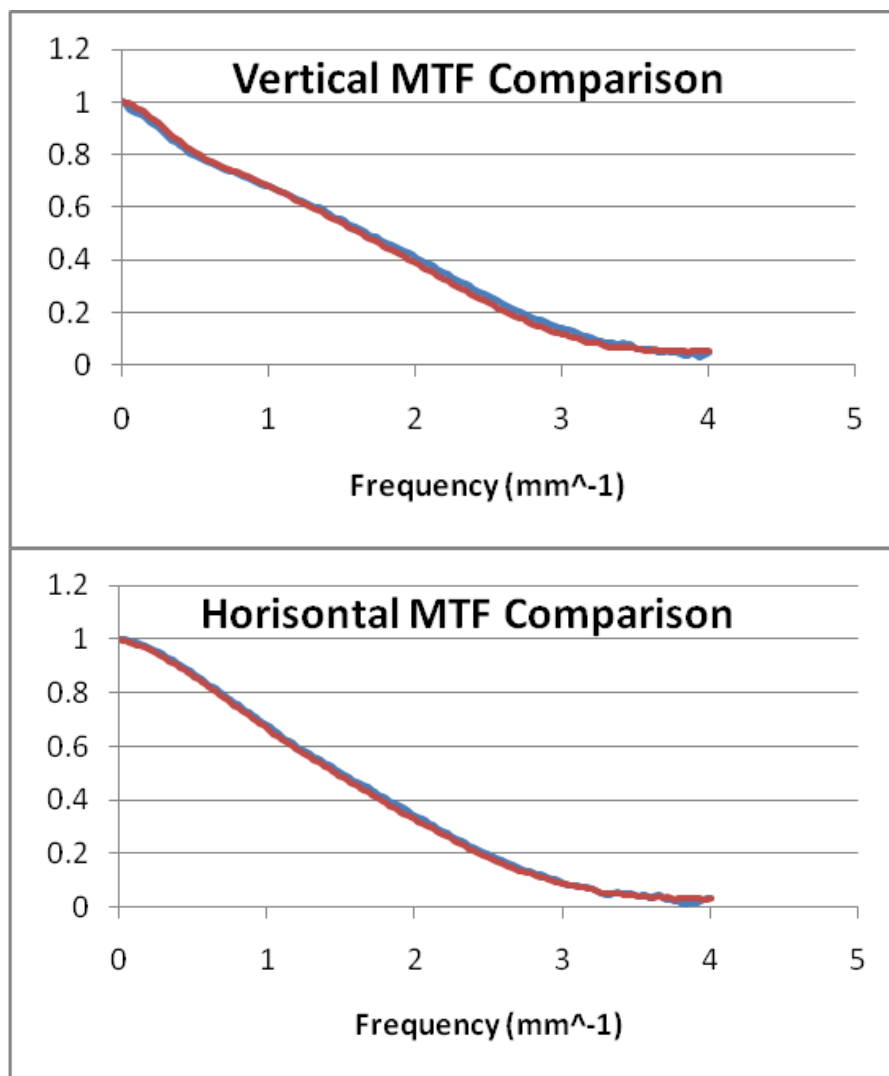
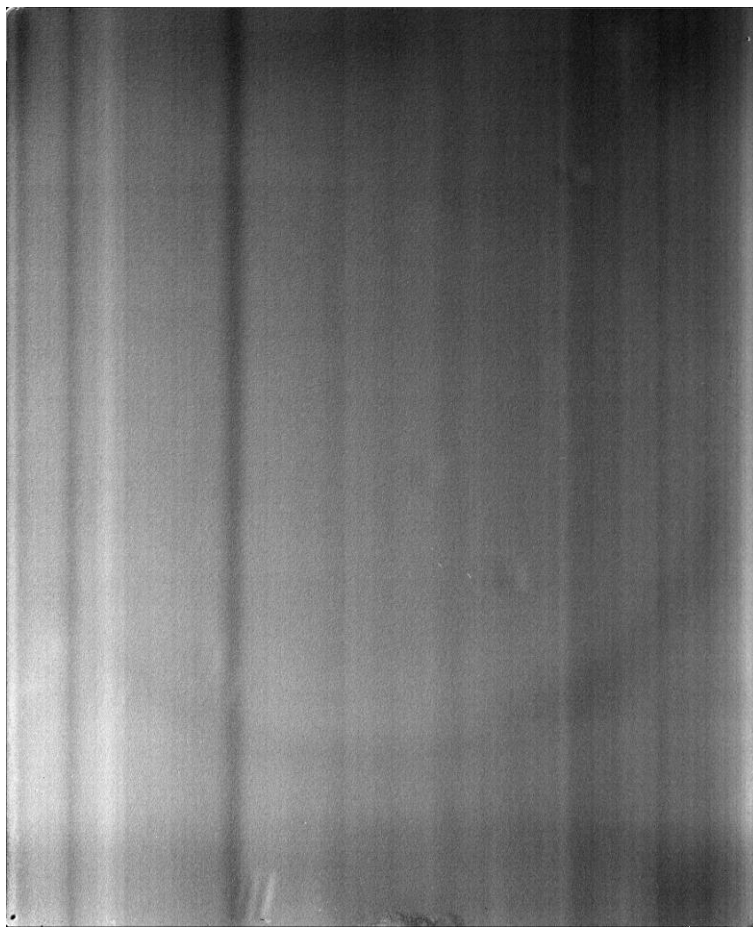


Figure 9: MTF comparison in the vertical and horizontal directions for single images (blue) and their corrected versions (red). Almost no variation is observed.

### *3.7 Variation across different readers*

The subtraction of images in figure 10 from the two readers reveals that there is some variation in scan artifacts across different readers. The window and level in the figure is optimized to show the structure, but the real variation is only on the order of one percent.



**Figure 10: Subtraction of images taken at 140kVp and 42mR without filtration, read out on different readers of the same make, model, and condition. The important structural difference arising from the reader variation is the vertical streaks resulting from differences in the horizontal scan.**

The image noise is different primarily in the horizontal direction, the direction of the laser scan. The gain map corrected image in figure 11 shows that the result will contain remnant artifacts after the correction if the gain map was produced on a different reader than the image.

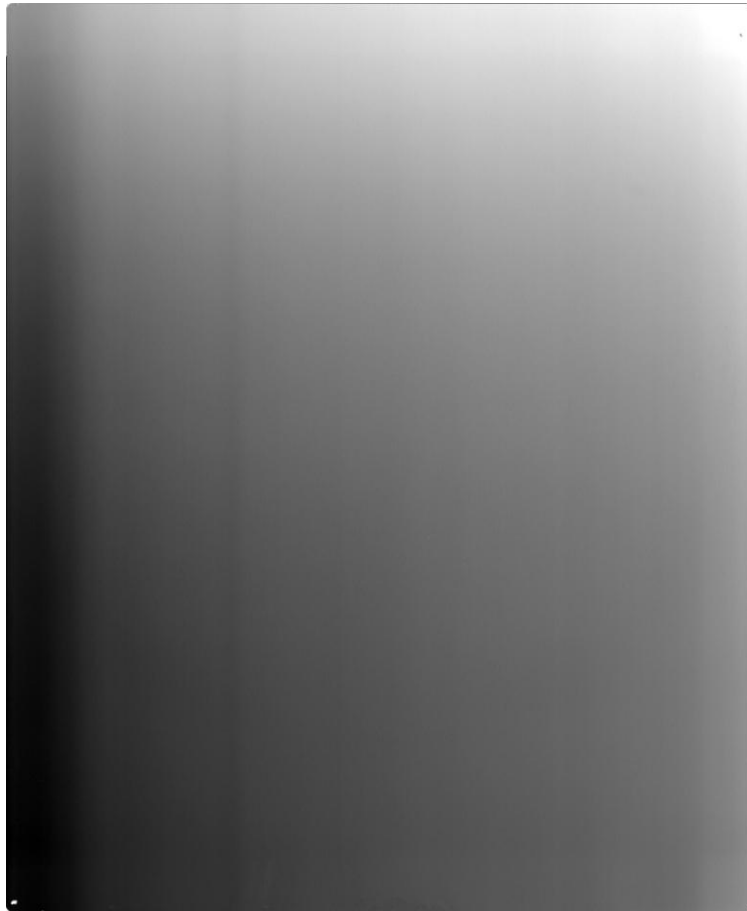


**Figure 11: Image taken at 140kVp, 42mR, no filtration, read out on the secondary reader. Correction made with gain map generated on the primary reader. Variation in scan artifacts causes some vertical streaking to remain.**

The less vertically uniform low frequency artifacts and horizontal artifacts seen in figure 1 are still largely removed from the image.

The noise power spectrum for the corrected and uncorrected image, in the horizontal direction, can be seen in figure 12. The low frequency artifacts are still effectively removed, but the mid range and high frequency noise is actually worsened by the correction, with the worst effect occurring at about  $1 \text{ mm}^{-1}$ .

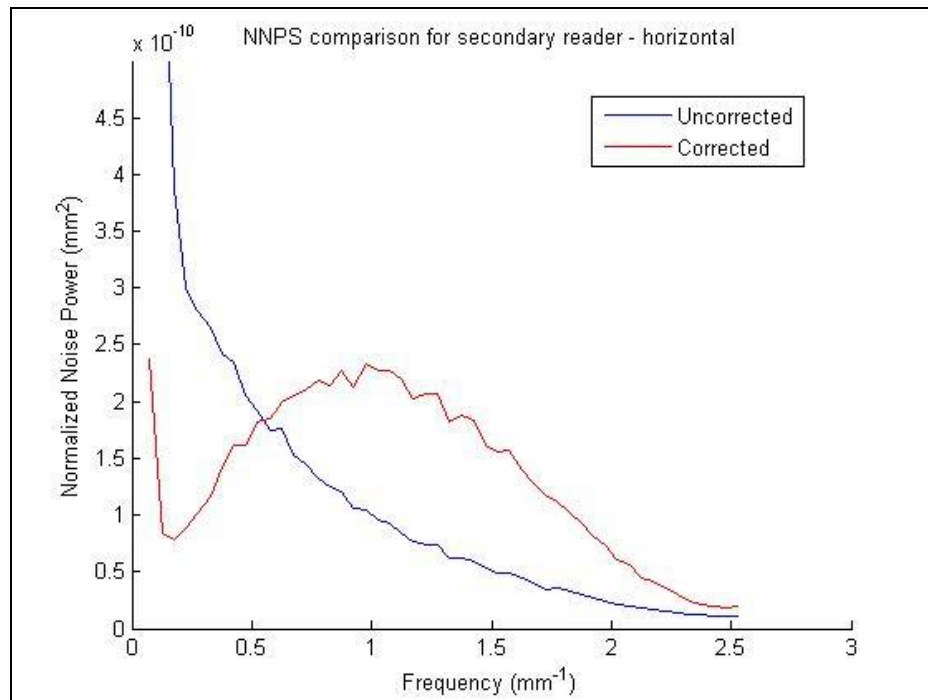


**Figure 12: Normalized noise power spectrum comparison in the horizontal direction between a corrected and uncorrected image read on the secondary reader. Image was acquired at 140kVp 42mR with no filtration. Correction was performed with gain map acquired on the primary reader. Notice correction of low frequency artifacts and noise while medium and high frequency noise is actually enhanced.**

The vertical normalized noise power spectrum comparison in the vertical direction is much closer to the results on the primary machine. The comparison, seen in figure 13, shows improvement across all frequencies, with the best improvement at low frequencies and the worst at high frequencies, as seen before.

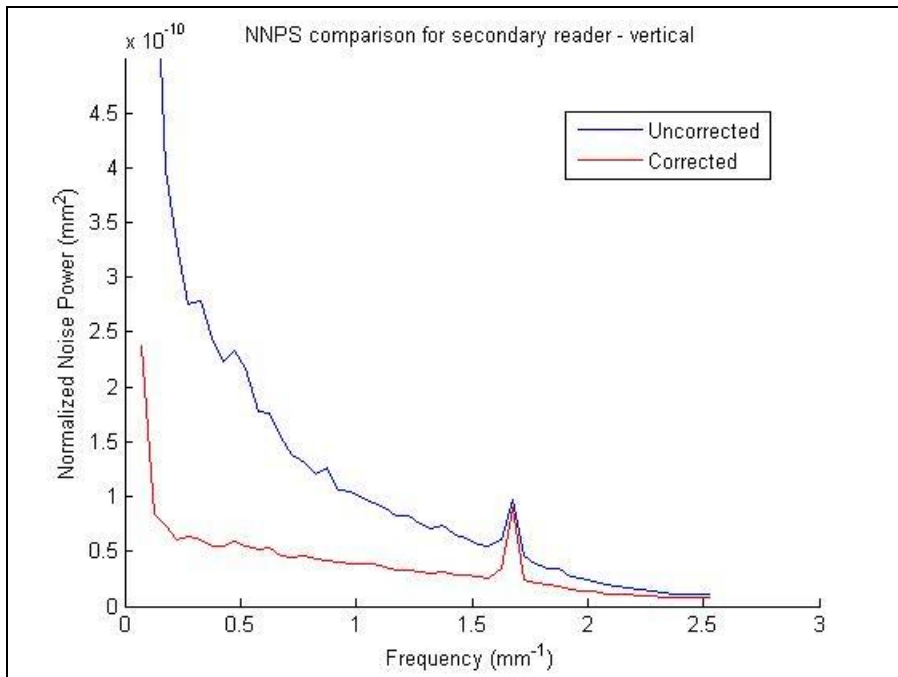


**Figure 13: Normalized noise power spectrum comparison in the vertical direction between a corrected and uncorrected image read on the secondary reader. Image was acquired at 140kVp 42mR with no filtration. Correction was performed with gain map acquired on the primary reader. Improvement is similar to same-reader analysis.**

## 4. Discussion

Computed radiography continues to be a viable clinical modality commonly used in many hospitals across the country as a digital, portable solution for bedside imaging due to the expense of the “gold standard” flat panel detectors. Despite this, little work has been done to improve the main limitation of CR: its image quality. The success of this work as a proof of concept that it is possible to apply quality improvement techniques to CR despite the apparent difficulty in such an endeavor will hopefully encourage further work in the area to maintain CR as a viable clinical option. That being said, there are still a number of elements in our process which could benefit from refinement.

The process by which the gain map is generated does a good job isolating the fixed pattern noise from the detector in the central region of the plate, but the filtration used yields some border effects which are undesirable. One thing that could be adjusted with this process is the shape of the kernel, the ideal being a Gaussian function to avoid “ringing” in frequency space as a result of the convolution. Additionally, while convolution is convenient, the edge mirroring method was not entirely effective in negating edge effects from using a very large kernel. Applying the filter directly in frequency space could aid in eliminating this issue, and the extra processing time would be insignificant, since gain map generation only needs to be performed once. The last optimization is the kernel size. While we know that a large kernel is needed for

filtration, the exact size which yields the best differentiation between fixed pattern noise from the plate and shading effects from the beam needs to be determined, and is likely specific to the x-ray tube used for delivery, as well as the beam parameters.

The evaluative program for NPS used is very strong, especially in the sense that it relates so well to the well understood measure of detector quality, DQE. Anticipated improvements on the system are related to its de-trending of background shading. The current form of the routine uses a ramp function to de-trend the background shading, but this is not entirely sufficient, and results in the spike at very low frequencies we see on the NNPS curves in figures 4, 7, and 8. Fitting a quadratic surface to the background shading in each ROI of the analysis will allow for more accurate NPS calculation at those frequencies.

Compensations for variations in the system in order to maximize the benefit of applying the Gain map are one of the main focuses of this work. The reduction in noise in the gain map itself through the averaging of images was very effective in nearing the asymptote for improvement in figure 8, and the fiducial system for alignment was able to align both the images contributing the gain map itself, and the images to be corrected, though the perceived change in NPS was not that large. Further, the practicality of having fiducial marks of some sort on the plate itself could be questioned. It creates a location without data in the image, and while essential information is not likely to be on the periphery, there is likely a better way. Some of our anticipated work is to develop a

fully computer based image analysis algorithm for alignment of images without the use of fiducials. Such a system would use small rotations and translations on the order of what we see using fiducial marks, and correct the base image after each transformation in an attempt to minimize some measure within the image, such as standard deviation in a flat region. A complication to this method would be the background shading, which is not corrected for. This shading could cause issues in the evaluation of the match.

Variations in tube voltage could also benefit from a similar correction. Figure 6 shows that the system has a varied response to different x ray energies. While the shape of the fixed pattern noise remains the same, the response in relation to the mean likely varies. As future progression on this project, we propose that an automatic scaling of the gain map could be used to optimize its performance at a variety of beam spectra. Such a system would scale the spread of the gain map about the unity mean while retaining that mean. This process could be done incrementally and evaluated at each step, finding the optimized spread which maximizes noise power reduction.

The largest contributor to the ability for this method to improve image quality is undoubtedly the exposure used to take the image. As we see in figure 5, there are vast differences between different orders of exposure. The ratio of fixed pattern noise to simple quantum noise in the image increases with exposure, which means that at low exposures less of the noise present in the image can be corrected for. Fixed pattern noise is also much more prevalent at low-to-mid frequencies, which is the reason medium and

low frequencies see such an increased benefit from correction. Clearly extremely high exposures would never be expected clinically on a patient, so the impressive gains we saw at 42mR would likely only be seen in industrial applications like non-destructive testing, but improvements can still be seen clinically. Average exposure for a CR image in the clinic is about 1mR, but it is important to note that this is an average. Areas of lower density, such as the lungs, would have greater exposure on the plate, and thus gain correction for those areas would be much stronger.

This system would be easy to implement clinically by the manufacturers. At the time of production, measurements could be made on the plate and a gain map generated immediately. This gain map could simply be included on some sort of media along with new plates from the manufacturer, or even available to be drawn from an online database, since plates all have a unique barcode sequence. The programming for the correction is all software based, and could likely be pushed in a software upgrade for the system. The hospital itself would need to do essentially no work to use the system, since it would be automated within the readout process. The only issue with implementation would be the generation of gain maps for plates already in clinical use, since they would last for some time in the clinic with their long lifespan.

We saw that the reader itself has some contribution to both the noise and artifact characteristics of CR images in the direction of motion of the scanning laser. This is likely due to differences in collection efficiency for the light guide across the plate. This

can often result from dust collection on the light guide itself. Since this contribution is included in the gain map with the process we used, using the gain map on a different reader can actually make the noise characteristics worse by correcting for a pattern which is not present. This could prove to be an obstacle to correction, especially at institution with multiple readers such as duke. One potential method for addressing this issue would be to generate a second correction specific to the reader which would address the contribution from the scanning system alone. The map could be generated by acquiring a large number of images at the same beam setting on different plates and the same reader, to hopefully average out any contribution from plate inhomogeneity. The reader specific map could then be used to remove scanner noise information from the plate specific gain map and make it scanner independent. The effectiveness of the scanner correction would depend on the amount of variation in the scanner pattern over time, though it could be used to correct the gain map to be scanner independent regardless. Once the scanner correction is determined initially, it would be relatively simple to track changes in the pattern periodically.

## **5. Conclusion**

In conclusion, it was found that by applying gain map correction to computed radiography images in a variety of image conditions allowed significant improvement of the DQE by reducing the fixed pattern noise in the images, thus reducing the noise power spectrum. While some details of the programming implementation and scanner specificity need to be refined, the system provides a clear benefit and would be easily implemented in a clinical setting.

## Bibliography

- <sup>1</sup> Samei E, Flynn MJ, Reimann DA. *A method for measuring the presampled MTF of digital radiographic systems using an edge test device.* Med Phys. 1998 Jan;25(1):102-13.
- <sup>2</sup> JT Dobbins, DL Ergun, L Rutz, DA Hinshaw, H Blume, DC Clark, *DQE(f) of four generations of computed radiography acquisition devices.*, Medical physics, United States, vol. 22 no. 10 (October, 1995), pp. 1581-93
- <sup>3</sup> E Samei, NT Ranger, JT Dobbins 3rd, Y Chen, *Intercomparison of methods for image quality characterization. I. Modulation transfer function.*, Medical physics, vol. 33 no. 5 (May, 2006), pp. 1454-65
- <sup>4</sup> JT Dobbins 3rd, E Samei, NT Ranger, Y Chen, *Intercomparison of methods for image quality characterization. II. Noise power spectrum.*, Medical physics, vol. 33 no. 5 (May, 2006), pp. 1466-75
- <sup>5</sup> JT Dobbins, *Image quality metrics for digital systems.* In *Handbook of Medical Imaging, Vol. 1, Van Metter RL, Beutel J, Kundel H (eds), SPIE Press, Bellingham, WA, 2000.*
- <sup>6</sup> IEC 61267 *Medical Diagnostic X-ray equipment – Radiation conditions for use in the determination of characteristics* 2005
- <sup>7</sup> Samei EJ, Flynn MJ, Chotas HG, Dobbins JT III, *DQE of direct and indirect digital radiography systems.* Proc. SPIE Medical Imaging 2001 Symposium, 4320:189-197, 2001
- <sup>8</sup> Ranger NT, Mackenzie A, Honey ID, Dobbins JT III, Ravin CE, Samei E, *Extension of DQE to include scatter, grid, magnification, and focal spot blur: a new experimental technique and metric.* Proc. SPIE Medical Imaging 2009 Symposium 7258:1A1-1A12, 2009
- <sup>9</sup> Maidment ADA, Albert M, Bunch PC, Cunningham IA, Dobbins JT III, Gagne RM, Nishikawa RM, Wagner RF, Van Metter RL: *Standardization of NPS measurement: interim report of AAPM TG16.* Proc. SPIE Medical Imaging 2003 Symposium, 5030:523-532, 2003
- <sup>10</sup> Rivetti S, Lanconelli N, Bertolini M, Nitrosi A, Burani A, Acchiappati D. *Comparison of different computed radiography systems: physical characterization and contrast detail analysis.* Med Phys. 2010 Feb;37(2):440-8.

- <sup>11</sup> Samei E, Ranger NT, MacKenzie A, Honey ID, Dobbins JT 3rd, Ravin CE. *Effective DQE (eDQE) and speed of digital radiographic systems: an experimental methodology*. Med Phys. 2009 Aug;36(8):3806-17.
- <sup>12</sup> Friedman SN, Cunningham IA. *A small-signal approach to temporal modulation transfer functions with exposure-rate dependence and its application to fluoroscopic detective quantum efficiency*. Med Phys. 2009 Aug;36(8):3775-85.
- <sup>13</sup> Vedantham S, Karellas A. *Modeling the performance characteristics of computed radiography (CR) systems*. IEEE Trans Med Imaging. 2010 Mar;29(3):790-806.